Mobilization of Entrapped Organic Fluids by Elastic Waves and Vibrations

Pavel P. Iassonov and **Igor A. Beresnev,** Iowa State University

Summary

The organic fluids entrapped in pore constrictions by capillary forces can be mobilized by the application of elastic-wave vibrations because of the nudging effect, which allows quantitative description. The model used for such calculations is a single-pore channel with converging/diverging geometry, in which the organic phase is entrapped as a continuous blob occupying several adjacent pores. The ganglion is released from the constriction when the wave-acceleration amplitude exceeds a threshold value that scales with the frequency as $A/f =$ a constant. This means that the wave intensity is the only required criterion for the release. In an ensemble of ganglia, the percentage of them mobilized and, therefore, the flow rate increases with the amplitude and decreases with frequency. The vibrations are inefficient for mobilization if the frequency is sufficiently high. The typical vibratory amplitudes required to produce noticeable increases in the average flow rates are on the order of 10 m/s^2 and much higher at the frequencies in excess of approximately 10 Hz. These estimates provide guidelines for the possible applications of elastic-wave stimulation of organic-fluid flow in porous environments.

Introduction

A great deal of attention in recent years has been devoted to the possibility of enhanced petroleum recovery using elastic waves and vibrations (Beresnev and Johnson 1994, Hilpert et al. 2000, Roberts et al. 2001 and 2003, Dobronravov 2002, Poesio et al. 2002). Nonetheless, the difficulty of the method has been insufficient understanding of the physical mechanism by which the low-frequency vibrations could mobilize the entrapped organic fluids. Hilpert et al. (2000) calculated the frequencies of pulsing pressure in an axisymmetric channel with a sinusoidal profile that maximized the volume of the displaced nonwetting phase; however, no explicit mobilization criteria were established. Several studies recently have proposed a specific oil-release mechanism showing how vibrations overcome capillary entrapment that holds the fluids in place (Graham and Higdon 2000, Iassonov and Beresnev 2003, Beresnev et al. 2005), which allowed explanation of miscellaneous observations of the enhancement in organic-phase flow by vibrations under field and laboratory conditions. This mobilization mechanism, as summarized by Beresnev et al. (2005), can be represented as follows.

The conditions for the capillary entrapment of nonwetting fluids in pores of variable diameter (the so-called Jamin effect) of course have been understood since the 1930s (Taber 1969). The residual fluids are immobilized in the form of isolated blobs (ganglia) because of an excess capillary pressure (P_c^+) building up on the inner side of the downstream meniscus as it enters a narrow pore constriction, relative to the upstream meniscus (P_c^-) (water-wet porous media will be assumed) (Payatakes 1982). Referring to **Fig. 1,** the oil ganglion can move if the absolute pressure in the oil at the left meniscus ($P_w^+ + \Delta P_w + P_c^-$) is greater than that at the right meniscus ($P_w^+ + P_c^+$), where P_w is the pressure in the water phase and $P_c^{\pm}$ is the capillary pressure determined from the Laplace equation. Equating the two leads to $\Delta P_{0w} = P_c^+ - P_c^-$ as the threshold external pressure drop in the water above which the ganglion is mobile (Taber 1969). It follows that the external gradient in the surrounding water needs to exceed a certain unplugging threshold ∇P_{0w} to carry the ganglion through (Taber 1969, Melrose and Brandner 1974).

This process is represented schematically on a flow-force diagram in **Fig. 2.** The solid line depicts the oil-phase flow for various values of the external static forcing. Under an external gradient $\nabla P_{sw} < \nabla P_{0w}$, the system resides in static equilibrium. The flow can commence only when ∇P_{sw} exceeds the unplugging threshold ∇P_{0w}.

Suppose that the flow is plugged ($\nabla P_{sw} < \nabla P_{0w}$). In a cylindrical channel, the application of longitudinal vibrations of the wall (without a loss of generality, we consider the motion parallel to the pore axis) is equivalent to the addition of an external (inertial) oscillatory body force P_{osc} to the constant gradient,

$$P_{\text{osc}} = \rho_p a, \quad \ldots\ldots\ldots\ldots\ldots (1)$$

where ρ_p is the density of the oil (petroleum) and a is an instantaneous amplitude of the acceleration of the wall (Biot 1956). One period of the oscillatory forcing adding to the gradient is shown in Fig. 2. When this forcing acts along the gradient and the total $\nabla P_{sw} + P_{\text{osc}}$ exceeds ∇P_{0w}, instant unplugging occurs (total forcing in the flow zone in Fig. 2). During the unplugged period, if a ganglion's leading meniscus moves beyond the narrowest point in the constriction, the magnitude of the restraining capillary force starts to decrease progressively. As a result, the blob accelerates upon exiting the constriction (Beresnev et al. 2005). This explains why the application of the reversed polarity of vibrations, opposing the gradient, cannot return the blob to its original position. The minimum amplitude for the vibrations needed to mobilize the blob is set by the condition $\nabla P_{sw} + P_{\text{osc}} > \nabla P_{0w}$.

Because the leading meniscus must reach the throat of the constriction to become mobilized, the period of vibrations should be long enough (for a given amplitude) to allow sufficient time for this movement. Frequencies above a certain threshold value will fail to mobilize the blob. We infer that, in addition to the existence of the minimum-amplitude threshold for the onset of mobilization, there will also be a maximum-frequency threshold.

This mechanism of residual-organic-phase mobilization by elastic waves and vibrations allows quantitative description of the flow-enhancement effect produced by seismic waves of particular amplitudes and frequencies, which would be of direct practical interest and has so far been lacking. Performing such calculations is the goal of this paper.

Model Formulation

Geometry of the Pore Channel. The model we consider is a capillary tube of circular cross section with the radius varying with length as

$$R(z) = \frac{1}{2}\left\{(r_{\max} + r_{\min}) + (r_{\max} - r_{\min})\cos\left(\frac{2\pi z}{l_{\text{pore}}}\right)\right\}, \quad \ldots\ldots (2)$$

where z is the axial coordinate, $r_{\min}$ and $r_{\max}$ are the minimum (pore-throat) and maximum (pore-body) radii of the channel, and l_{pore} is the length of a single pore (Fig. 1). This model represents a periodic structure of pore elements with converging/diverging geometry, capturing the crucial factor responsible for the capillary entrapment of nonwetting fluids in porous space. The following values of channel geometry will be used: $r_{\min} = 0.025$ mm, $r_{\max} = 0.05$ mm, and $l_{\text{pore}} = 0.5$ mm.

Original SPE manuscript received for review 30 March 2006. Revised manuscript received for review 13 March 2008. Paper (104315) peer approved 30 May 2008.

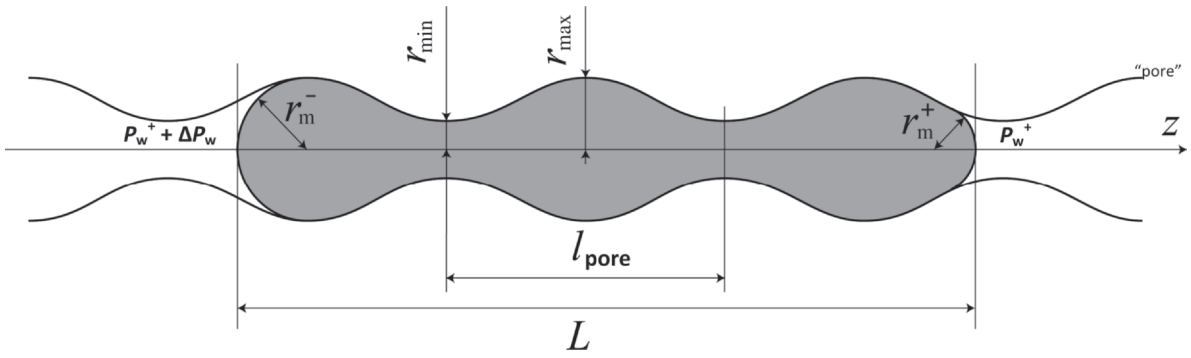

Fig. 1—Geometry of the model pore channel and entrapped oil blob.

Modeling Vibrations. To simulate the effect of vibrations, we use the oscillating body force P_{osc} (Eq. 1) acting on the fluid. The volume-average value of this force is

$$P_{osc} = (A\rho_p)\cos(2\pi ft), \quad \ldots\ldots\ldots\ldots\ldots\ldots\ldots\ldots\ldots\ldots (3)$$

where A and f are the acceleration amplitude (hereafter simply referred to as the amplitude) and the frequency of vibrations, respectively. For the density of the pore-filling fluid, a typical value for crude oil of 800 kg/m^3 will be assumed.

Interfaces and Capillary Forces. The ganglion of nonwetting fluid (oil) is represented by a finite volume of oil situated within the pore channel, bound at both ends by water/oil interfaces (menisci) (Fig. 1). The interfaces are assumed to be spherical, with the radius of curvature uniquely defined by the position of the contact line on the pore wall and the contact angle. This assumption is valid only in the quasistatic case, the validity of which is addressed in the next subsection. A zero-contact angle will be assumed (complete water-wetting of the wall, with oil being the nonwetting fluid), and the contact-angle hysteresis will not be considered.

Under these conditions, the capillary pressures P_c on the inner (blob) side of each meniscus at any given moment are

$$P_c^{\pm} = \frac{2\sigma}{r_m^{\pm}}, \quad \ldots\ldots\ldots\ldots\ldots\ldots\ldots\ldots\ldots\ldots\ldots\ldots\ldots\ldots (4)$$

where σ is the surface tension (the value of $\sigma = 20$ mN/m will be used) and r_m is the radius of curvature of the meniscus (Fig. 1).

We postulate that the length of the blob L is significantly greater than the length of a single pore l_{pore}. In this case, the end effects (such as the flow in the vicinity of the interfaces) can be neglected in calculating the dynamics of the entire blob.

Quasistatic Approach. We apply a quasistatic approach to the solution (i.e., treat the flow within the model at any time as steady-state). The limits of applicability of this assumption can be seen if we consider the problem of a startup flow in a circular channel (Johnson 1998). The flow in response to a step forcing approaches its steady state over a characteristic time scale that is often called the viscous-diffusion time,

$$\tau_{vd} = \frac{\rho r^2}{\mu}, \quad \ldots\ldots\ldots\ldots\ldots\ldots\ldots\ldots\ldots\ldots\ldots\ldots\ldots\ldots (5)$$

where r is the radius of the channel and μ is the dynamic viscosity. Substituting the maximum radius of 0.05 mm and fluid viscosity $\mu = 5$ mPa·s, we obtain the viscous diffusion time of 0.0004 seconds. This value should be significantly smaller than the scale of any time-dependent process in the model, which in our case is vibration. For the highest vibratory frequency we use (40 Hz), the period of vibration T is 0.025 seconds. We see therefore that the condition $\tau_{vd} \ll T$ is always satisfied, justifying the use of the quasistatic approach.

The time scale (Eq. 5) can also be construed as the characteristic response time of the fluid to a vibratory forcing. Vibrations with $T \ll \tau_{vd}$ will simply fail to affect the fluid because the fluid will not have sufficient time to respond.

The quasisteady approach allows us to calculate the oil-flow rate at any given moment on the basis of the conductivity C of the channel, which will generally depend on the system geometry and the current position of the interfaces. For $L \gg l_{pore}$, we can neglect the effects of the menisci position on the conductivity and calculate the oil-flow rate Q_p as an analog of Poiseuille flow with a vibrational body force added. The absolute-pressure difference between the oil side at the left and right menisci in Fig. 1, driving the ganglion in the positive direction of the z-axis, is $(P_w^+ + \Delta P_w + P_c^-) - (P_w^+ + P_c^+) = \Delta P_w + P_c^- - P_c^+$, where $(P_w^+ + \Delta P_w) - P_w^+$ is the external-pressure drop in the water phase. The same analogy is used to derive the Washburn equation for the rate of capillary rise (Dullien 1992). Assuming a constant pressure gradient, dividing by L, and adding the external body force P_{osc} leads to

$$Q_p = \frac{C}{\mu_p}\left(-\frac{dP_w}{dz} + \frac{P_c^- - P_c^+}{L} + P_{osc}\right), \quad \ldots\ldots\ldots\ldots\ldots\ldots (6)$$

where the conductivity depends only on the geometry of a single pore, $\frac{dP_w}{dz}$ is the external-pressure gradient in the surrounding water phase (the negative pressure gradient drives the fluid in the positive direction of the z-axis in Fig. 1), and P_{osc} is the oscillatory body force (Eq. 3). Note that the pressure differences in both the oil and water phases have entered the derivation of Eq. 6. Because

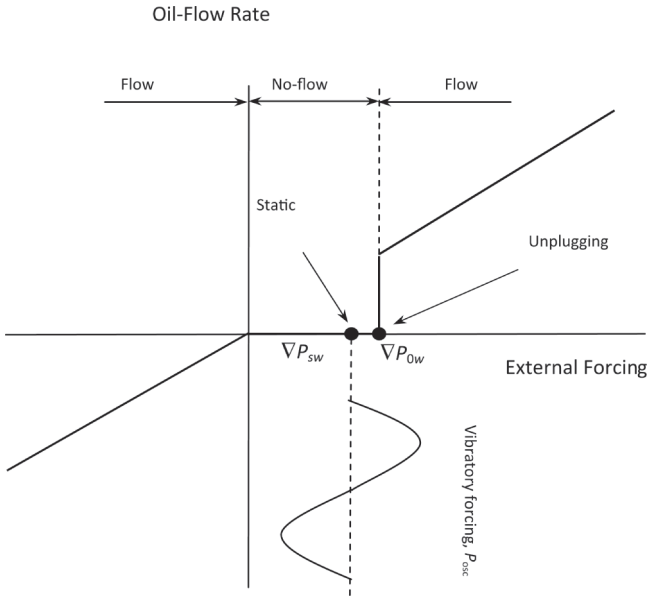

Fig. 2—Mechanism of the mobilization of entrapped organic ganglion under the combined effect of external-pressure gradient and oscillatory forcing.

of the assumption of a long blob and the resulting applicability of Poiseuille flow, only the oil viscosity controls the flow rate.

In the absence of vibratory forcing, $Q_p = 0$ when $-\mathrm{d}P_w/\mathrm{d}z = (P_c^+ - P_c^-)/L$, which is the condition for entrapment of Taber (1969). The flow resumes when $-\mathrm{d}P_w/\mathrm{d}z$ exceeds this value.

The value of C was calculated numerically with the computational fluid-dynamics code Fluent™ (www.fluent.com). Using a steady-state axisymmetric laminar-flow solver for the geometry of a single pore (Eq. 2), and applying a pressure difference between the inlet and the outlet of the pore, we obtained the single-phase flow rate, which in turn was used to calculate the value of the conductivity $C = 4.44 \times 10^{-19}$ m^4.

To justify the use of a constant conductivity, we also must ensure that the flow in the channel is laminar at any time. This can be achieved by calculating the Reynolds number (Johnson 1998)

$$N_{\mathrm{Re}} = \frac{\rho_p V_p D}{\mu_p}, \qquad (7)$$

where V_p is the maximum oil velocity and D is the diameter of the channel. Assuming the parabolic (Poiseuille) velocity profile, V_p can be calculated as twice the average fluid velocity in the narrowest part of the pore,

$$V_p = 2\frac{Q_p}{\pi r_{\min}^2}. \qquad (8)$$

In naturally occurring porous media, the turbulence may be observed for Reynolds numbers as low as 1 (Fetter 2001). Using Eqs. 8, 7, and 6, we calculate that, to achieve Re = 1, we would need to apply a pressure gradient of approximately 10^6 Pa/m (hereafter, we refer to the absolute value of the pressure gradient for simplicity). This value is very high and cannot be achieved in a typical oilfield environment, except in close proximity to the well. Our assumption of the laminar flow, therefore, is justified for the types of applications we are considering.

Algorithm of Flow Calculation. From Eq. 6, the flow in the model depends on the three types of forces acting on the blob: the external pressure gradient $\frac{\mathrm{d}P_w}{\mathrm{d}z}$, the capillary pressures on oil/water interfaces inside the blob $P_c^\pm$, and the oscillating body force P_{osc} caused by vibration. As follows from the entrapment criterion, for an arbitrary external-pressure gradient in the absence of vibration, the oil flow is plugged as long as

$$-\frac{\mathrm{d}P_w}{\mathrm{d}z} < \frac{P_c^+ - P_c^-}{L}. \qquad (9)$$

Considering that the right side of Eq. 9 will vary with the menisci position, this equation assumes the maximum capillary pressure difference $P_c^+ - P_c^-$ for all possible positions of the blob for its given volume. This allows finding the static pressure gradient needed to mobilize a particular oil blob, as well as the equilibrium position of the menisci for any pressure gradient that is not sufficient to mobilize the oil.

If the ganglion is mobile, we can calculate the flow rate with Eq. 6. The calculations then proceed in time in a stepwise manner. Knowing the current flow rate, we calculate the positions and curvatures of the interfaces at the next time step, accounting for the change in the cross section of the channel (Eq. 2) and the change in radius of the menisci. An adaptive timestep selection algorithm is employed, requiring that the timestep be significantly smaller than the period of vibration and, at any given step, that the capillary pressure not change by greater than a predefined threshold (typically, less than 2.5%).

The following criteria were used to determine the result of each simulation. The oil ganglion was considered immobile if its leading interface had not advanced beyond its last known maximum position (along the pore axis z) for several periods of vibration. The actual number of cycles considered varied from simulation to simulation. Typically, though, the majority of entrapped ganglia were either mobilized in only one or two periods or remained immobile. The ganglion was considered mobile if the leading interface had traveled a distance of one pore length or greater (because of periodic structure of the pore, this is a sufficient condition). Each simulation time could be limited by these criteria and provide a simple yes/no answer, saying whether the oil was mobile or not under the applied initial conditions. In the case of the average-flow calculation, the mobilization criterion was modified slightly in that the required movement of the interface was extended to several pore lengths in order to improve the precision of the result.

Results and Discussion

Presenting Results of Simulations. As seen in Eq. 9, in the case of no vibration, the mobilization of the blob is simply a matter of creating a sufficient pressure difference,

$$\Delta P_{0w} = \frac{\mathrm{d}P_w}{\mathrm{d}z} L, \qquad (10)$$

by the external gradient. It follows that, for a given gradient, the longer ganglia will be mobile while the shorter ones will not (Payatakes 1982). Also, the pressure difference required for the mobilization will be an approximately periodic function of L (or the ganglion volume) because the resisting capillary pressure imbalance $P_c^+ - P_c^-$ is periodic with period l_{pore}. This behavior can be seen in **Fig. 3,** where the threshold difference ΔP_{0w} is plotted against the ganglion volume varying over one pore element. The fate of the ganglion, therefore, will depend highly on slight variations in the ganglion volume within one pore. This variability should be accounted for properly in the representation of the flow-mobilization phenomenon.

A meaningful way of characterizing the fate of the blob (and quantifying the mobilizing effect of vibration) on a macroscopic level would then be to define it not for a ganglion of any particular volume (or length) but for an ensemble of ganglia occupying the range of lengths from $L - l_{\mathrm{pore}}/2$ to $L + l_{\mathrm{pore}}/2$. In the following, we use the fraction of mobile ganglia over all ganglia in the ensemble. An example of such a calculation is presented in **Fig. 4,** where the fraction of mobile blobs is plotted vs. the external-pressure gradient. Each point on the curve is the value for an ensemble of 1,000 blobs with the macroscopic length of $L = 10$ cm increasing in uniform increments over one pore element. All ganglia are mobile when the gradient exceeds the maximum capillary pressure difference $P_c^+ - P_c^-$ calculated for all lengths.

Amplitude Effect. This method and the statistical measure introduced can be used to calculate the effect of vibration on the mobilization of ganglia in the model. Since almost any pressure gradient would be sufficient to mobilize a certain fraction of blobs of particular length (Fig. 4), we assume in the following that, before the start of vibrations, only immobile ganglia remain in the porous medium, representing the residual-oil saturation. It then becomes convenient to calculate the fraction of mobilized ganglia [i.e., the number that have become mobilized as a result of vibratory stimulation (M_A) normalized by the total number of ganglia immobile under the given pressure gradient without vibrations (M_0)],

$$M^* = \frac{M_A}{M_0}. \qquad (11)$$

This result is shown in **Fig. 5,** where M^* is plotted vs. amplitude for several values of pressure gradient. As in Fig. 4, each data point represents an ensemble of 1,000 volumes of the blobs with $L = (10 \pm 0.5\ l_{\mathrm{pore}})$ cm. The stimulation frequency is 10 Hz. It is seen that the mobilization effect grows with amplitude.

The curves in Fig. 5 are informative, yet they are insufficient to describe fully the vibratory mobilization because the effect will also depend on the frequency and the ganglion length.

Frequency Effect. As stated in the Introduction, the mobilizing effect of vibration, for a given amplitude, is expected to decrease with increasing frequency. Only those blobs in the ensemble for which the frequency is below the threshold value will be mobilized.

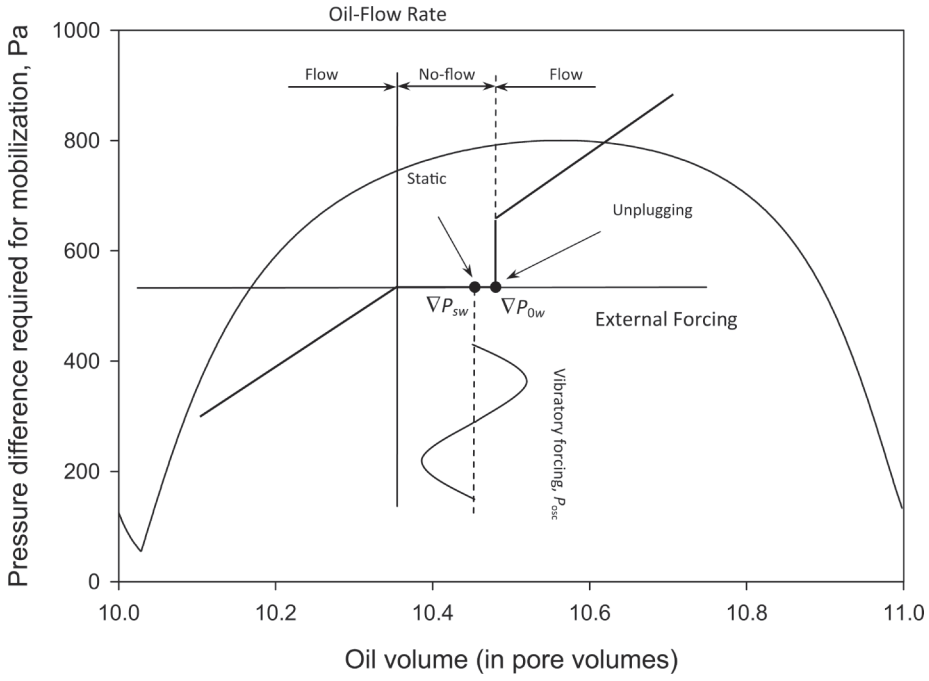

Fig. 3—The effect of oil-ganglion volume on pressure difference required for the mobilization.

Calculations corroborate the frequency dependence of the mobilization effect. It is demonstrated in **Fig. 6,** where the fraction of mobilized ganglia is plotted against frequency for several acceleration amplitudes A (the external gradient is 7050 Pa/m). Recall that, at the pressure gradient of 7050 Pa/m, 50% of the ganglia are trapped (Fig. 4). It is clear that the effect of vibration at a given amplitude A ranges from full mobilization (100%) to no mobilization (0%), depending on the frequency.

We also observe that, in the range of frequencies presented, the amplitude required to mobilize a set fraction of ganglia appears to increase almost linearly with the frequency. This dependence is better illustrated in **Fig. 7a,** where the amplitude required for the mobilization of a fraction of immobile oil is plotted against frequency. The linear relationship is easily explained. As we have pointed out, the blob's leading meniscus must be carried to the narrowest point of the constriction over one period of vibration in order to be mobilized; for a blob of a given volume, the required travel distance constitutes a certain fraction s of the length of the pore. If the blob's velocity is V_p, this leads to the mobilization condition $V_p\ T \approx s\ l_{\text{pore}}$. Since $V_p \sim A$, we obtain $A/f \sim s\ l_{\text{pore}} = \text{constant}$, which is the pattern seen in Fig. 7a.

It stands to reason that there are frequency limits within which this argument applies. At the high-frequency end, the linear dependence between the mobilizing amplitude and the frequency will hold as long as the condition of quasistatic approximation, $\tau_{vd} \ll T$, applies. At the other extreme, at sufficiently low frequencies, including zero (static mobilizing forcing), the distance traveled over one period will always exceed the length of the pore; as long as

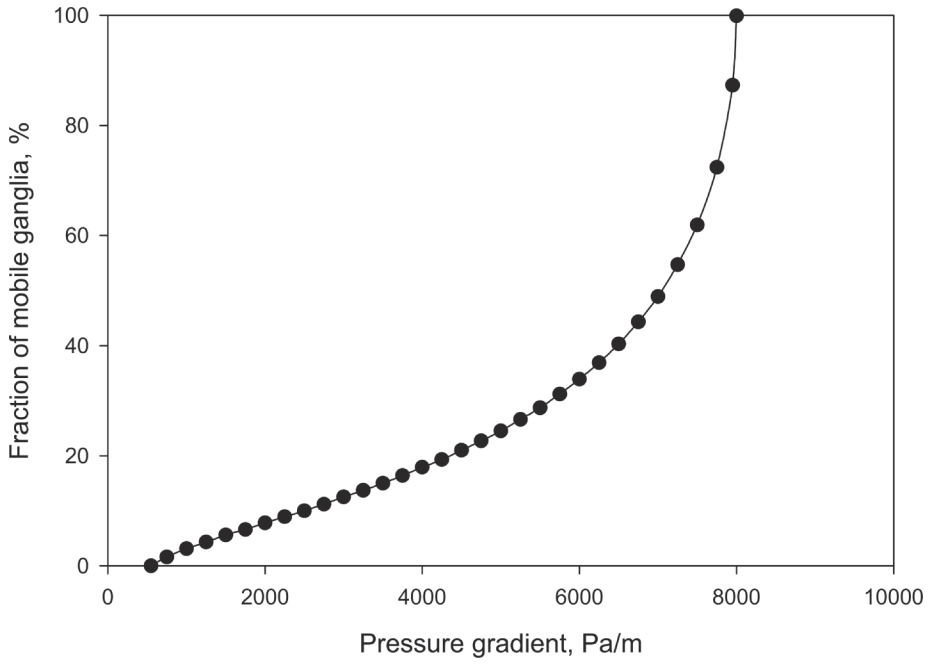

Fig. 4—The effect of external-pressure gradient on the mobilization of oil ganglia of length L=10 cm spanning the range of lengths within one pore element.

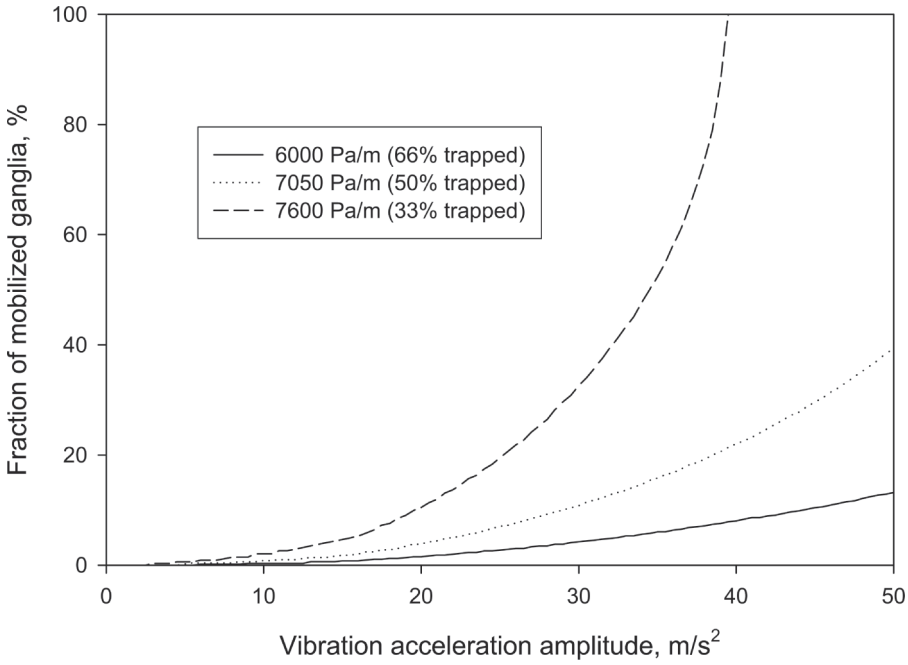

Fig. 5—The effect of vibration amplitude on the mobilization of oil ganglia of length *L*=10 cm. The frequency of vibrations is 10 Hz.

this is the case, the frequency effect will not be seen, and the linear dependence will level off at the value corresponding to the static mobilization forcing presented in Fig. 4. This behavior is demonstrated in Fig. 7b obtained from the calculations. It shows that the frequencies at which the leveling off occurs are extremely low (on the order of one-hundredth of a Hz; they will scale as l_{pore}^{-1}); for practical purposes, this deviation from the A/f = constant dependence could be ignored.

It follows that, in practice, one could conveniently characterize the effect of vibration with one parameter, A or f, knowing that a constant A/f leads to the same result. It is also important that this ratio is related directly to the sound intensity, a measure of the energy of the sonic wave used in acoustics,

$$I = \frac{\rho_s c}{8\pi^2}\left(\frac{A}{f}\right)^2, \quad \ldots\ldots\ldots\ldots\ldots\ldots\ldots\ldots\ldots\ldots\ldots\ldots\ldots\ldots\ldots\ldots (12)$$

where ρ_s is the density of the solid and c is the wave-propagation velocity. We then infer that another, physically deeper-rooted, way of characterizing the effects of the amplitude and frequency would be to use the intensity measure: the mobilizing effect of the fields having the same intensity is the same. As follows from Fig. 7a, to increase the effect, the intensity must be increased.

Ganglion-Length and Pressure-Gradient Effects. The effect of the length of the entrapped ganglion on the mobilization, for a given gradient, will be to scale proportionally the required amplitude (intensity), as can be understood from Fig. 2 and Eq. 9. Considering that the maximum $P_c^+ - P_c^-$ is approximately the same for every length, a decrease in L will result in an increase in the right side of Eq. 9 and, thus, in moving the static gradient ∇P_{sw} away from the mobilization threshold ∇P_{0w} in Fig. 2. Conse-

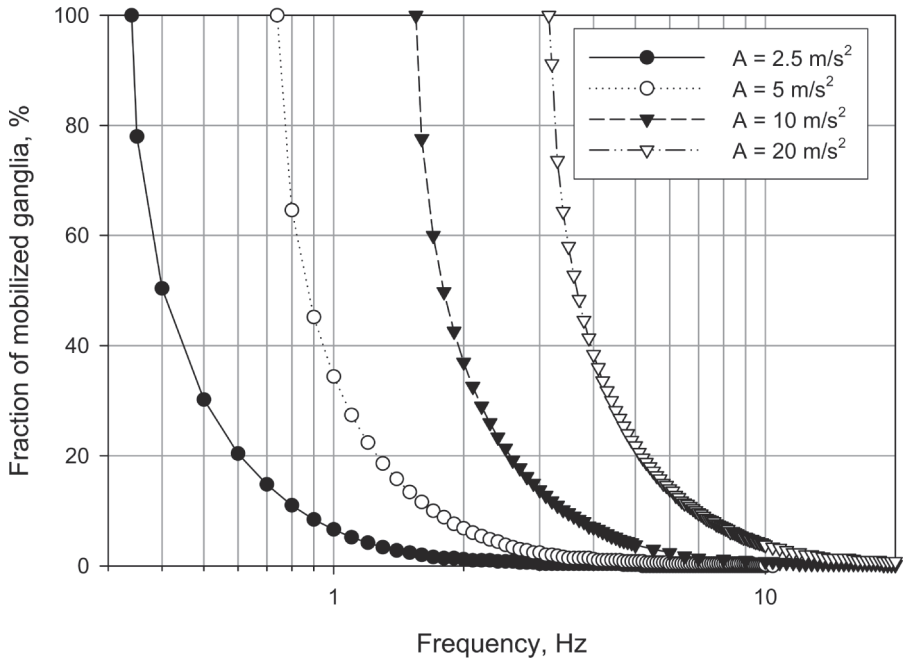

Fig. 6—The effect of vibratory frequency on the mobilization of ganglia (*L*=10 cm) for several amplitudes under the external-pressure gradient of 7050 Pa/m.

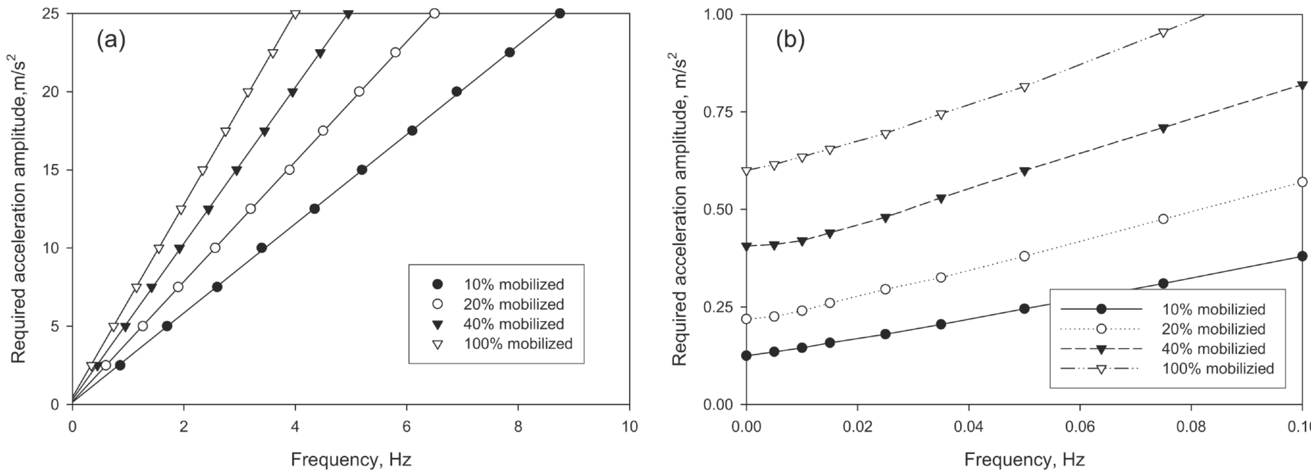

Fig. 7—The amplitude and frequency effect on the mobilization of entrapped ganglia (L=10 cm; $\left|\frac{dP_w}{dz}\right|$=7050 Pa/m).

quently, a proportionally larger P_{osc} will be needed to unplug the ganglion. Similarly, at larger pressure gradients and given L, the same effect will be achieved at proportionally smaller vibration amplitudes (intensities).

Vibration Effect on Flow Rate. We have so far discussed the vibratory effect on the mobilization of oil ganglia. From the practical standpoint, it is also important to characterize the effect of vibrations on the flow rate, which, for example, could be used to predict an absolute increase in organic-fluid production. We again present these results in terms of the mean flow rates, averaged over oil ganglia with lengths changing in the range $L \pm l_{pore}/2$.

The dependence of the average flow rate on the pressure gradient (with no vibrations applied) for an oil blob of length $L=10$ cm is shown in **Fig. 8.** To emphasize the stimulating effect of vibrations, it is convenient to normalize the enhanced flow rate (with the vibrations applied) by that without vibrations, representing a relative increase in Q_p,

$$Q_p^* = \frac{Q_{Ap} - Q_{0p}}{Q_{0p}}, \qquad (13)$$

where Q_{Ap} is the rate under the vibrations with amplitude A and Q_{0p} is the rate without vibrations. This result is shown in **Fig. 9,** where Q_p^* is plotted against the external gradient for different values of A. Clearly, the relative mobilization effect increases with amplitude. The peaks observed in the curves can be understood as follows: For any given amplitude, the flow rate increases with the increasing gradient as more and more blobs from the ensemble become mobilized and start to flow. However, clearly, at the combination of amplitude and gradient at which nearly all of the blobs are already mobile, there is no possibility to increase the flow rate any further, and the curve quickly drops to zero.

The effect of frequency on the flow rate will understandably be controlled by the ratio A/f, as was the case for the fraction of mobilized ganglia in Fig. 7a. This dependence is illustrated in **Fig. 10.** The same flow-rate increase is achieved for a constant value of the ratio.

Estimation of Realistic Seismic Effects. It would be interesting to estimate the magnitude of residual-oil-mobilization effect that could be expected under realistic field conditions. According to the data available to the authors and from the authors' experience, the

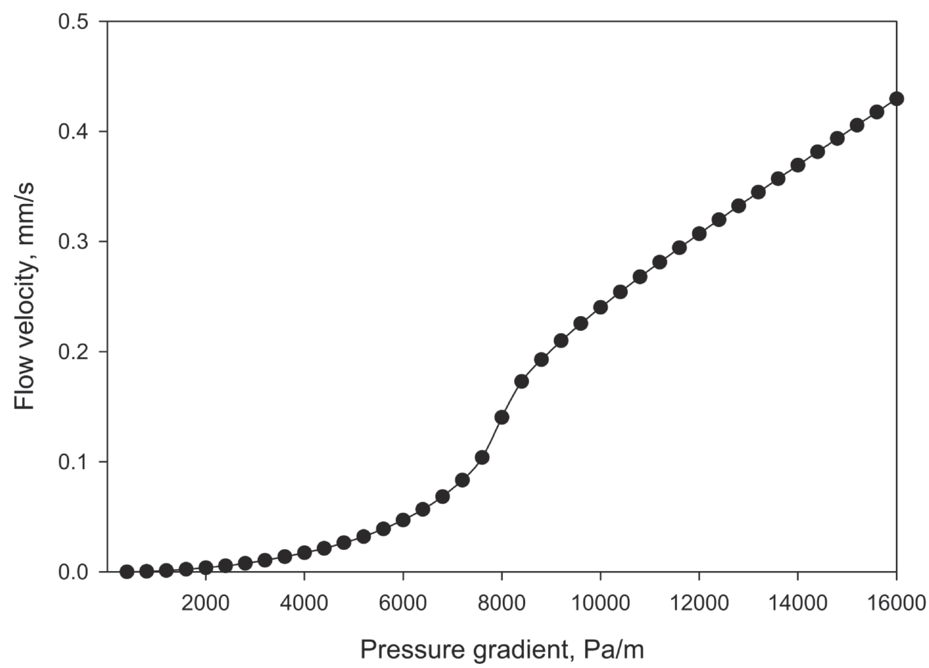

Fig. 8—The effect of external-pressure gradient on the average flow rate for the ganglia of L=10 cm spanning the range of lengths within one pore element.

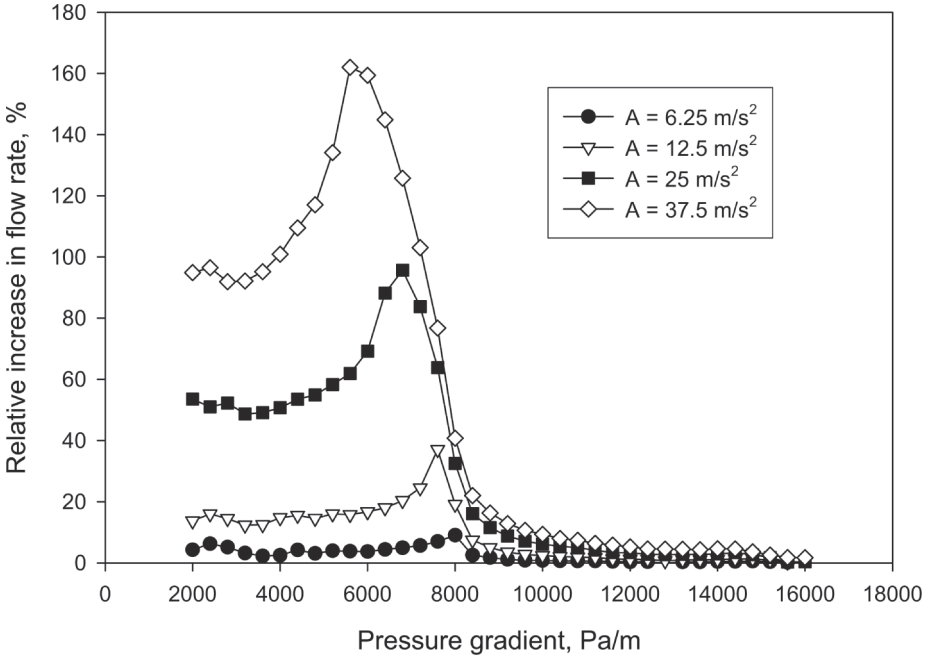

Fig. 9—The increase in the average flow rate as a result of application of vibration with various amplitudes. The frequency is 10 Hz.

existing nonexplosive borehole seismic-energy sources are capable of creating maximum displacements at a distance of ~300 m on the order of 10^{-6} m at the central frequency of ~100 Hz, providing an estimate of maximum acceleration of ~0.4 m/s^2. According to Fig. 6, the mobilization effect at such amplitudes and frequencies could be expected to be negligibly small except for the volume of the reservoir immediately surrounding the borehole. We infer that much more powerful sources would be needed to stimulate reservoir volumes within a few hundred meters. It is not within the purview of this paper to suggest how this technically could be achieved. It stands to reason, though, that a significant stimulation effect could be achieved with the use of surface vibrators to stimulate the near-surface flow, which has direct implications for the remediation of groundwater contaminated by entrapped organic fluids (e.g., leaking gasoline tanks).

It should be noted that the conclusion about the magnitude of accelerations needed to achieve a sizeable oil-recovery effect is based on the model of entrapped-fluid liberation by vibrations considered in this paper. If other mechanisms of liberation are in play, the estimate of the required amplitudes possibly may be relaxed. For example, Nikolaevskiy (2006) hypothesizes that seismic waves in reservoir rock induce oscillations and friction between grains that in turn produce ultrasound. Ultrasound releases the gas dissolved in the oil to form microbubbles; the bubbles stick to the oil droplets and cause their flotation. The mechanism considered in our paper does not take this possible phenomenon into account.

The mobilizing effect of ultrasonic waves with the frequency of 20 kHz in a sandstone core saturated with brine/residual oil was recently reported by Tu et al. (2007). When the sound intensity

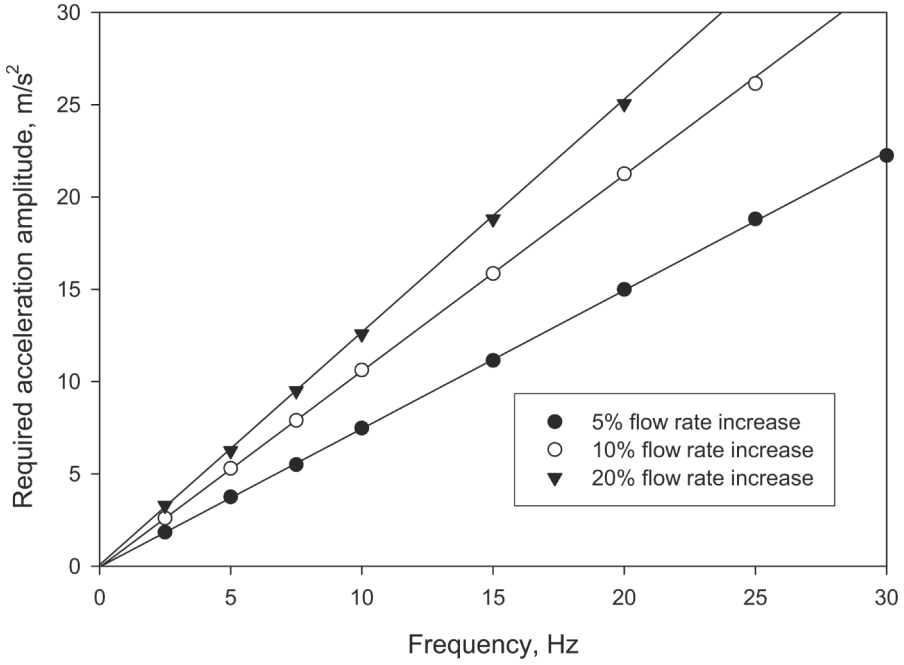

Fig. 10—The amplitude and frequency effect on the average flow rate of oil ganglia (L=10 cm; $\left|\frac{dP_w}{dz}\right|$=7050 Pa/m).

exceeded a certain threshold, the residual oil started to exude from the sample. Because of the jump-like dependence on the intensity, the authors did not attribute this effect to changes in interfacial or fluid properties by ultrasonic action. Qualitatively, this observation is in line with the inference from our model that the amplitude needs to surpass a prescribed threshold to liberate the oil. However, a step-like increase in the oil mobility when the threshold is exceeded would be the case only for a single ganglion. While, for an ensemble of blobs, (and channels with varying geometry), each having its own threshold, a more gradual increase in the residual-oil production (such as the one seen in Fig. 5) would rather be expected, which was not observed by Tu et al. (2007). At this time, it is difficult for us to explain their single observation. On the other hand, the frequency of 20 kHz used, although seemingly high, is still realistic to produce a tangible mobilization effect within the model considered. Assuming a pore radius of 0.01 mm for a natural sandstone and the density and viscosity as previously noted, we obtain $\tau_{vd} \approx 2\ 10^{-5}$ seconds. The period of ultrasound is $T = 5\times10^{-5}$ seconds, showing that these two quantities are comparable and the oil would have had sufficient time to respond to vibrations. From this standpoint, the effect observed by Tu et al. (2007) is entirely plausible even without the ultrasound changing the fluid properties. However, estimating the amplitude needed to initiate the stimulation, based on the mobilization condition $\nabla P_{sw} + P_{\mathrm{osc}} > \nabla P_{0w}$, would be interesting but is not currently possible because of the absence of pore-size information.

Hamida and Babadagli (2007) also reported an increase in oil-recovery rate from oil-saturated rock samples in the presence of a 40-kHz ultrasound. They, however, explain the results by the ultrasonic waves decreasing the interfacial tension between the oleic and surrounding aqueous phase and reducing the films adsorbed on pore walls, in line with the respective mechanisms reviewed by Beresnev and Johnson (1994). Our present model deals with low-frequency vibrations that do not change fluid properties and is not applicable to the results reported in Hamida and Babadagli (2007).

Conclusions

We presented a model for approximate calculation of the effect of vibration on the mobilization and average flow of oil blobs in pore channels of variable radii, representing realistic converging/diverging geometry of the naturally occurring porous media.

The calculated effects of the amplitude and frequency agree with the expectations from the mobilization mechanism presented in Fig. 2. For a particular entrapped blob, there is a minimum amplitude required for its mobilization. This amplitude scales linearly with the frequency so that the ratio A/f is kept constant. At a given amplitude, if the frequency becomes sufficiently high, the mobilizing effect of vibrations stops altogether. We should mention, however, that this statement applies only within the applicability limits of the model, detailed in the Quasistatic Approach subsection. At higher frequencies, other mechanisms, such as reduction in the effective capillary force caused by change in the menisci shape or breakup of ganglia, may result in certain mobilization effects. Other possible phenomena unaccounted for (Nikolaevskiy 2006) may also lead to mobilization at perhaps lower amplitudes.

In terms of practical applications, this model can be used to estimate absolute volumes of oil mobilized by given amplitudes and frequencies of vibration, provided sufficient information on pore-size and ganglia-size distribution in the porous reservoir is available. It also provides the minimum amplitude and maximum allowable frequency required to initiate the stimulation effect.

The calculations show that, for the parameters of the model corresponding to typical oil-bearing formations, the vibratory amplitudes required to achieve noticeable mobilization and increase in the oil-flow rate are rather high (e.g., Figs. 6 and 9), on the order of at least 10 m/s^2, and are much higher at frequencies in excess of 10 Hz, which is not realistically achievable by the available borehole seismic sources. The goal of the low-frequency stimulation of large volumes of oil reservoirs thus seems beyond the reach of the existing technical means, unless significant increases in the output elastic-wave energies of seismic sources are obtained. This, however, does not apply to the possibility of vibratory stimulation of near-surface contaminated aquifers, in which necessary sonic energies can be created from the surface.

Our model deals with a single pore channel and does not incorporate the interconnectivity of real porous media. Nevertheless, interconnectivity can be argued to favor the release of entrapped ganglia compared to a single channel of the same average geometry. Indeed, if an oil ganglion occupies a large number of pores, some of the downgradient menisci will likely be closer to the mobilization threshold than the meniscus of the average channel; the mobilization will then occur through that more-susceptible throat. In this sense, our model can be viewed as an upper-bound estimate for the respective mobilizing parameters of the vibratory fields. Similar treatment of multiple-pore ganglia in interconnected pore systems, which would require complete characterization of (still poorly understood) dynamic behavior of menisci as they invade a node of several pores, is yet to be provided. That task is left for the future.

Nomenclature

A = acceleration amplitude
a = amplitude of wall acceleration
C = conductivity
D = diameter
I = sound intensity
L = length
l_{pore} = length of pore
N_{Re} = Reynolds number
P_c = capillary pressure
P_{osc} = oscillatory body force
P_w = pressure in water phase
Q_p = oil-flow rate
r = radius
r_m = radius of curvature of meniscus
r_{max} = pore-body radius
r_{min} = pore-throat radius
V_p = maximum oil velocity
μ = dynamic viscosity
ρ_p = oil density
ρ_s = solid density
σ = surface tension
τ = time

Acknowledgments

This work was supported by the National Science Foundation and the Petroleum Research Fund. Acknowledgment is made to the donors of the American Chemical Society Petroleum Research Fund for their generosity. We are grateful to W. Deng, R. Ewing, D. Vigil, and W. Li for stimulating discussions. The article benefited from reviews and suggestions by V.N. Nikolaevskiy and three anonymous referees.

References

Beresnev, I.A. and Johnson, P.A. 1994. Elastic-stimulation of oil production: A review of methods and results. *Geophysics* **59** (6): 1000–1017. DOI:10.1190/1.1443645.

Beresnev, I.A., Vigil, R.D., Li, W., Pennington, W.D., Turpening, R.M., Iassonov, P.P., and Ewing, R.P. 2005. Elastic waves push organic fluids from reservoir rock. *Geophys. Res. Lett.* **32** (L13303). DOI:10.1029/2005GL023123.

Biot, M.A. 1956. Theory of propagation of elastic waves in a fluid-saturated porous solid. II. Higher frequency range. *J. Acoust. Soc. Am.* **28** (2): 179–191. DOI:10.1121/1.1908241.

Dobronravov, O.V. 2002. Industry feature: A new technology of reservoir stimulation through exposure to weak seismic waves. *First Break* **20** (6): 376–382. DOI:10.1046/j.1365-2397.2002.00287.x.

Dullien, F.A.L. 1992. *Porous Media: Fluid Transport and Pore Structure*. San Diego, California: Academic Press.

Fetter, C.W. 2001. *Applied Hydrogeology*, fourth edition. Upper Saddle River, New Jersey: Prentice Hall.

Graham, D.R. and Higdon, J.J.L. 2000. Oscillatory flow of droplets in capillary tubes. Part 2. Constricted tubes. *J. Fluid Mech.* **425:** 55–77. DOI:10.1017/S0022112000002032.

Hamida, T. and Babadagli, T. 2007. Analysis of capillary interaction and oil recovery under ultrasonic waves. *Transport in Porous Media* **70** (2): 231–255. DOI:10.1007/s11242-006-9097-9.

Hilpert, M., Jirka, G.H., and Plate, E.J. 2000. Capillarity-induced resonance of oil blobs in capillary tubes and porous media. *Geophysics* **65** (3): 874–883. DOI:10.1190/1.1444784.

Iassonov, P.P. and Beresnev, I.A. 2003. A model for enhanced fluid percolation in porous media by application of low-frequency elastic waves. *J. Geophys. Res.* **108** (B3): 2138. DOI:10.1029/2001JB000683.

Johnson, R.W. ed. 1998. *The Handbook of Fluid Dynamics*. Boca Raton, Florida: CRC Press.

Melrose, J.C., and Brandner, C.F. 1974. Role of capillary forces in determining microscopic displacement efficiency for oil recovery by waterflooding. *Journal of Canadian Petroleum Technology* (October–December): 54–62.

Nikolaevskiy, V.N. 2006. Vibrate—Seismic waves can change oil-gas reservoir state. In *Innovations in Nonlinear Acoustics: ISNA 17: 17th International Symposium on Nonlinear Acoustics Including the International Sonic Boom Forum*, ed. A.A. Atchley, V.W. Sparrow, and R.M. Keolian, 157–166. Melville, New York: AIP Conference Proc., American Institute of Physics.

Payatakes, A.C. 1982. Dynamics of oil ganglia during immiscible displacement in water-wet porous media. *Ann. Rev. Fluid Mech.* **14:** 365–393. DOI:10.1146/annurev.fl.14.010182.002053.

Poesio, P., Ooms, G., Barake, S., and van der Bas, F. 2002. An investigation of the influence of acoustic waves on the liquid flow through a porous material. *J. Acoust. Soc. Am.* **111** (5): 2019–2025. DOI:10.1121/1.1466872.

Roberts, P.M., Esipov, I.B., and Majer, E.L. 2003. Elastic wave stimulation of oil reservoirs: Promising EOR technology? *The Leading Edge* **22** (5): 448–453. DOI: 10.1190/1.1579578.

Roberts, P.M., Sharma, A., Uddameri, V., Monagle, M., Dale, D.E., and Steck, L.K. 2001. Enhanced DNAPL transport in a sand core during dynamic stress stimulation. *Environmental Engineering Science* **18** (2): 67–79. DOI:10.1089/10928750151132230.

Taber, J.J. 1969. Dynamic and Static Forces Required To Remove a Discontinuous Oil Phase From Porous Media Containing Both Oil and Water. *SPEJ* **9** (1): 3–12. SPE-2098-PA. DOI: 10.2118/2098-PA.

Tu, X., Ooms, G., and van der Bas, F. 2007. Experimental evidence of ultrasonic stimulation of brine-oil flow through a porous rock in laboratory conditions. *Transport in Porous Media* **70** (3): 323–333. DOI: 10.1007/s11242-007-9102-y.

Pavel Iassonov holds a PhD degree in geophysics from Iowa State University. **Igor Beresnev** is a professor of geophysics at Iowa State University. His interests include fluid dynamics, exploration geophysics, and earthquake seismology. Beresnev holds an MS degree from Moscow State University and a PhD degree from the Institute of Physics of the Earth, Russian Academy of Sciences, both in geophysics.